Antiviral Research 84 (2009) 205–214

Contents lists available at ScienceDirect

Antiviral Research

journal homepage: www.elsevier.com/locate/antiviral

Solution characterization of [methyl-^{13}C]methionine HIV-1 reverse transcriptase by NMR spectroscopy☆

Xunhai Zheng, Geoffrey A. Mueller, Eugene F. DeRose, Robert E. London*

Laboratory of Molecular Biophysics, MR-01, National Institute of Environmental Health Sciences, NIH, Research Triangle Park, NC 27709, United States

ARTICLE INFO

Article history:
Received 25 March 2009
Received in revised form 15 June 2009
Accepted 30 July 2009

Keywords:
HIV-1 reverse transcriptase
Solution behavior
[Methyl-^{13}C]methionine labeled
NMR spectroscopy

ABSTRACT

HIV reverse transcriptase (RT) is a primary target for drug intervention in the treatment of AIDS. We report the first solution NMR studies of [methyl-^{13}C]methionine HIV-1 RT, aimed at better understanding the conformational and dynamic characteristics of RT, both in the presence and absence of the non-nucleoside RT inhibitor (NNRTI) nevirapine. The selection of methionine as a structural probe was based both on its favorable NMR characteristics, and on the presence of two important active site methionine residues, $M184_{66}$ and $M230_{66}$. Observation of the M184 resonance is subunit dependent; in the p66 subunit the solvent-exposed residue produces a readily observed signal with a characteristic resonance shift, while in the globular p51 subunit, the $M184_{51}$ resonance is shifted and broadened as M184 becomes buried in the protein interior. In contrast, although structural data indicates that the environment of M230 is also strongly subunit dependent, the M230 resonances from both subunits have very similar shift and relaxation characteristics. A comparison of chemical shift and intensity data with model-based predictions gives reasonable agreement for $M184_{66}$, while $M230_{66}$, located on the β-hairpin "primer grip", is more mobile and solvent-exposed than suggested by crystal structures of the apo enzyme which have a "closed" fingers-thumb conformation. This mobility of the primer grip is presumably important for binding of non-nucleoside RT inhibitors (NNRTIs), since the NNRTI binding pocket is not observed in the absence of the inhibitors, requiring instead that the binding pocket be dynamically accessible. In the presence of the nevirapine, both the $M184_{66}$ and $M230_{66}$ resonances are significantly perturbed, while none of the methionine resonances in the p51 subunit is sensitive to this inhibitor. Site-directed mutagenesis indicates that both M16 and M357 produce two resonances in each subunit, and for both residues, the intensity ratio of the component peaks is strongly subunit dependent. Conformational features that might explain the multiple peaks are discussed.

Published by Elsevier B.V.

1. Introduction

HIV-1 reverse transcriptase (RT) has emerged as a central target for drug intervention in the treatment of AIDS (Autran et al., 1997; Tachedjian and Goff, 2003). RT plays a pivotal role in HIV replication by converting single-stranded genomic RNA into double-stranded proviral DNA. The enzyme catalyzes two reactions: DNA polymerization and RNA hydrolysis. It is composed of two subunits, p66 and p51, with both active sites located in the p66 subunit. The catalytic conversion of single-stranded viral RNA into double-stranded DNA requires that RT binds successively to a series of four distinct primer/templates combinations: tRNA/RNA, DNA/RNA, RNA/DNA and DNA/DNA. In order to accommodate this range of substrate structures, the enzyme must exhibit substantial conformational flexibility. The conformational variability of HIV reverse transcriptase is particularly well illustrated by its interactions with non-nucleoside RT inhibitors (NNRTI) (Das et al., 2007; Ren et al., 1995, 2001; Tachedjian and Goff, 2003). Formation of the NNRTI binding pocket requires extensive conformational rearrangement of the apo enzyme. The inhibitory effect has been proposed to result from combinations of three potential contributions: (1) direct distortion of the catalytic site; (2) interference with the hinge region of the protein that connects the palm and thumb subdomains, referred to as the "arthritic thumb" model (Shen et al.,

Abbreviations: DSS, 2,2-dimethylsilapentaned-5-sulfonic acid; HEPT, 1-[(2-hydroxyethoxy)methyl]-6-(phenylthio)thymine; IPTG, Isopropyl thio-D-galactoside; HSQC, heteronuclear single-quantum coherence; NNRTI, non-nucleoside RT inhibitors; NMR, nuclear magnetic resonance; NOE, nuclear Overhauser effect; pdb, Protein Data Bank; RMSD, root mean square deviation; RT, reverse transcriptase.

☆ This research was supported by the Intramural Research Program of the National Institute of Environmental Health Sciences, National Institutes of Health. Dr. DeRose's contribution was funded in whole with Federal funds from NIH/NIEHS, under delivery order HHSN273200700046U to SRA International, Inc.

* Corresponding author at: NIEHS, 111 T. W. Alexander Drive, PO Box 12233, Research Triangle Park, NC 27709, United States. Tel.: +1 919 541 4879; fax: +1 919 541 5707.
E-mail address: london@niehs.nih.gov (R.E. London).

0166-3542/$ – see front matter. Published by Elsevier B.V.
doi:10.1016/j.antiviral.2009.07.021

2003; Tachedjian and Goff, 2003); (3) effects on heterodimer association constant (Tachedjian et al., 2001; Venezia et al., 2006). The behavior of the apo enzyme in solution has been of interest since crystal structures show that it adopts a closed, inactive conformation (Rodgers et al., 1995; Hsiou et al., 1996; Bauman et al., 2008). Alternatively, Esnouf et al. (1995) were able to crystallize RT in an open conformation in the presence of a low affinity NNRTI, which was subsequently soaked out of the crystal.

In the present study, we have utilized [methyl-^{13}C]methionine labeled RT in order to probe the conformational behavior of the enzyme in solution and to evaluate the response to the NNRTI inhibitor nevirapine (Kohlstaedt et al., 1992; Tachedjian and Goff, 2003). In addition to favorable motional properties that result in relatively sharp resonances, methionine is located at two critically important active site positions: the YMDD motif on the β9–β10 hairpin, and at the end of the β12–β13 primer grip hairpin (Wang et al., 1994; Ding et al., 1998; Powell et al., 1997; Gutierrez-Rivas and Menendez-Arias, 2001; Tachedjian et al., 2001). Additionally, the position of the M357 loop is sufficiently close to the dimer interface to be sensitive to dimer formation. The locations of these methionine residues make them ideal probes for monitoring dynamic and conformational perturbations induced by both nucleoside and non-nucleoside inhibitors.

2. Materials and methods

2.1. Materials

Oligonucleotides used as PCR primers for site-directed mutagensis were purchased from Integrated DNA Technologies. Unlabeled amino acids, Q-Sepharose FF and the ssDNA cellulose matrix were purchased from Sigma–Aldrich. [ε-^{13}C]Methionine was obtained from Cambridge Isotope Laboratories. Isopropyl thio-D-galactoside (IPTG) was from Invitrogen. HiLoad 26/60 Superdex 200 column was from Amersham Pharmacia Biotech AB.

The plasmids of pET21a (+) p66 and pET30a (+) p51 were a generous gift from Dr. Sam Wilson, NIEHS. We utilized no purification tags. The p51 construct terminates at W426. Mutation of each of the six methionines to leucine individually and in combination was carried out by using the QuickChange XL site-directed mutagenesis kit (Stratagene). The desired mutated gene sequences were confirmed by DNA sequence analysis. Expression was controlled by the T7/lac promoter, which carried ampicillin or kanamycin antibiotic resistance, respectively. The two expression plasmids were transformed into *E. coli* BL21 (DE3) codon plus RIPL, and the protein expression was induced by addition of IPTG into the culture. The purification procedure of all mutants of both RT and p51 subunit was the same as described below. Each of the mutants constructed of p51 and p66 is listed below:

Protein sample	Concentration (μM)
[Methyl-^{13}C]methionine$_{66}$ RT	57
[Methyl-^{13}C]methionine$_{51}$ RT	50
[Methyl-^{13}C]methionine$_{51}$ M357L$_{51}$ RT	39
[Methyl-^{13}C]methionine$_{66}$ M16L RT	80
[Methyl-^{13}C]methionine$_{66}$ M41L RT	50
[Methyl-^{13}C]methionine$_{66}$ M164L RT	80
[Methyl-^{13}C]methionine$_{66}$ M184L RT	35
[Methyl-^{13}C]methionine$_{66}$ M230L RT	60

2.2. Sample preparation

For the purpose of NMR studies, each subunit of RT was expressed at 37 °C using enriched medium (PAG) (Studier, 2005) containing 17 unlabeled amino acids (no C, Y and M), plus [ε-^{13}C]methionine, which is expected to repress the endogenous synthesis of methionine by the bacteria (Muchmore et al., 1989).

The cell pellets containing p66 and p51 were mixed and resuspended in buffer A (50 mM Tris–HCl, 5% Glycerol, 50 mM NaCl, 1 mM DTT, and 0.5 mM EDTA pH 8.0) and sonicated together. The suspension was centrifuged at 30,000 × *g* for 30 min. All purification procedures were performed at 4 °C. The clarified supernatant was loaded on a Q Sepharose FF column, and an ssDNA cellulose column connected in tandem. When the OD_{280} of the flow-through was observed to be stable for 1 h (approximately 100 ml of wash), the ssDNA cellulose column was washed with 50 mM to 1 M NaCl gradient of buffer A. The fractions containing both RT subunits were pooled based on SDS-PAGE analysis. The pooled fractions were concentrated to less than 5 ml, and loaded onto a HiLoad 26/60 Superdex-200 gel filtration FPLC column which was pre-equilibrated with 50 mM Tris–HCl 200 mM NaCl. The heterodimer could be cleanly separated from excess monomer with the Superdex 200. Because there was generally an excess of p51, this insured the correct ratio p51 to p66. The fractions, which contain both RT subunits in an apparent 1:1 ratio as verified by SDS-PAGE analysis, were pooled and concentrated with Amicon Ultra-15 centrifugal filter device (Millipore).

The final samples were exchanged into NMR buffer (10 mM Tris–HCl-d11, pD7.6, 200 mM KCl, 1.5 mM sodium azide, 4 mM $MgCl_2$, and 100 μM 2,2-dimethylsilapentaned-5-sulfonic acid (DSS) as an internal chemical shift standard, in D_2O) using a PD-10 desalting column (Pharmacia), and further concentrated to approximately 50 μM. The concentration of each sample was determined by u.v. absorbance.

2.3. NMR spectroscopy

All NMR experiments were performed at 25 °C using a Varian UNITY INOVA 500 MHz NMR spectrometer, equipped with a 5 mm Varian (500 MHz) ^{1}H{^{13}C, ^{15}N} triple-resonance cryogenically cooled probe, with actively shielded Z-gradients. We used the Varian gChsqc experiment included in Biopack with the phase-cycling option. The acquisition parameters for all experiments were 64 transients, 64 ms acquisition with 1024 points and sweep width of 14 ppm. In the indirect dimension, 128 points were acquired with a sweep width of 11 ppm, the ^{13}C offset was set to 17 ppm. All NMR data were processed using NMRPipe (Delaglio et al., 1995) and analyzed with NMRviewJ (Johnson and Blevins, 1994).

2.4. Nomenclature

Subscripts have been used to denote the subunit involved when there is any possibility of ambiguity, e.g., [methyl-^{13}C]methionine$_{51}$ RT refers to the methionine labeled p51 subunit, and M230$_{66}$ refers to the M230 residue in the p66 subunit.

3. Results

Each subunit of HIV-1 reverse transcriptase contains six methionine residues that are distributed as illustrated in Fig. 1. The apo enzyme is shown in a conformation in which the fingers and thumb adopt a closed conformation (Fig. 1a, pdb code: 3DLK) as well as a fingers–thumb open conformation (Fig. 1b, pdb code: 1RTJ). The two methionine-containing β-hairpins at the active site of the p66 subunit are shown in Fig. 1c. HIV-1 reverse transcriptase was prepared containing [methyl-^{13}C]methionine in either the p66 or p51 subunits using a parallel expression system (Hou et al., 2004). The labeled and unlabeled subunits are combined immediately upon cell lysis and the RT heterodimer is subsequently purified. Fig. 2a shows the ^{1}H–^{13}C HSQC spectrum of 57 μM HIV-1 RT prepared to contain [methyl-^{13}C]methionine in the p66 subunit. We will refer to this species as [methyl-^{13}C]methionine$_{66}$ RT. Resonances were assigned using site-specific M → L mutants, with the results for the

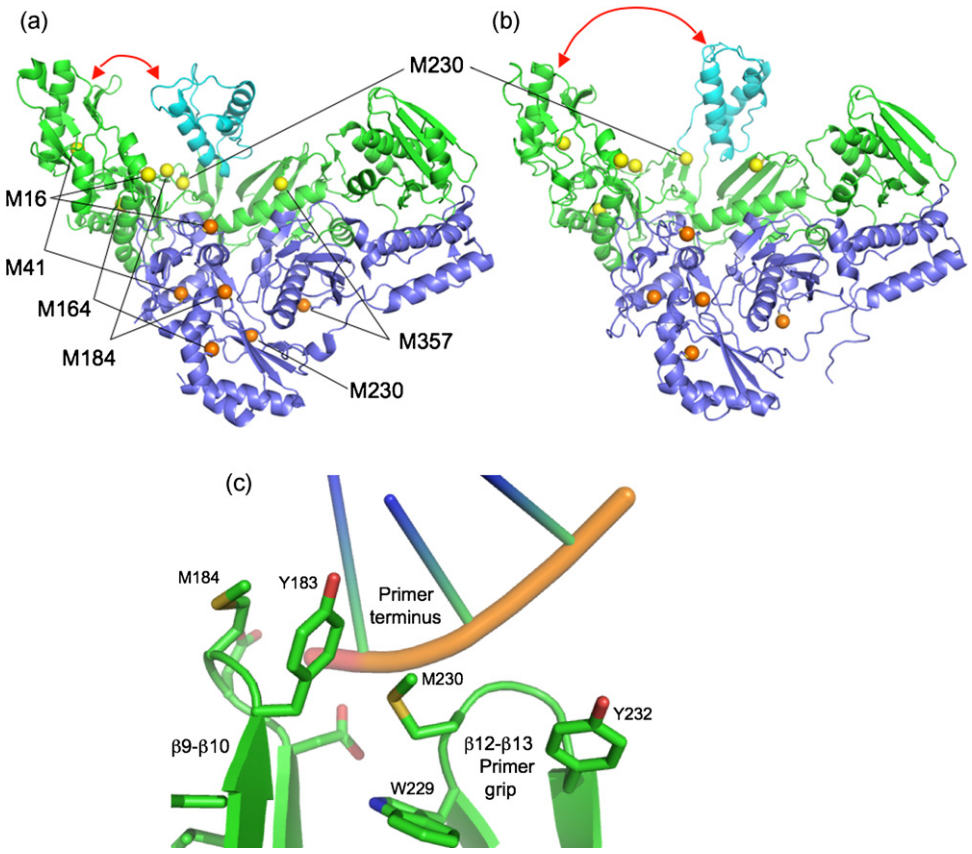

Fig. 1. Methionine residue positions in apo RT structures. (a) apo RT in a conformation in which the relative orientation of fingers and thumb is closed. The figure was based on pdb code 3DLK, and apo RT structures 1DLO and 1HMV adopt a similar, closed conformation. (b) apo RT in an open conformation (pdb code 1RTJ). The p51 subunit is shown in blue, the p66 subunit in green, except for the thumb domain of the p66 subunit, which is shown in cyan. Methionine residues of the p66 and p51 subunits are indicated as yellow and orange spheres, respectively. (c) The two methionine-containing β-hairpins corresponding to the active site YMDD motif (β9–β10 hairpin), and to the primer grip (β12–β13 hairpin) are illustrated (based on pdb file 1HYS). The proximity of M184 to Y183 is consistent with the upfield ^{1}H shift for M184 Cε. (For interpretation of the references to color in this figure legend, the reader is referred to the web version of the article.).

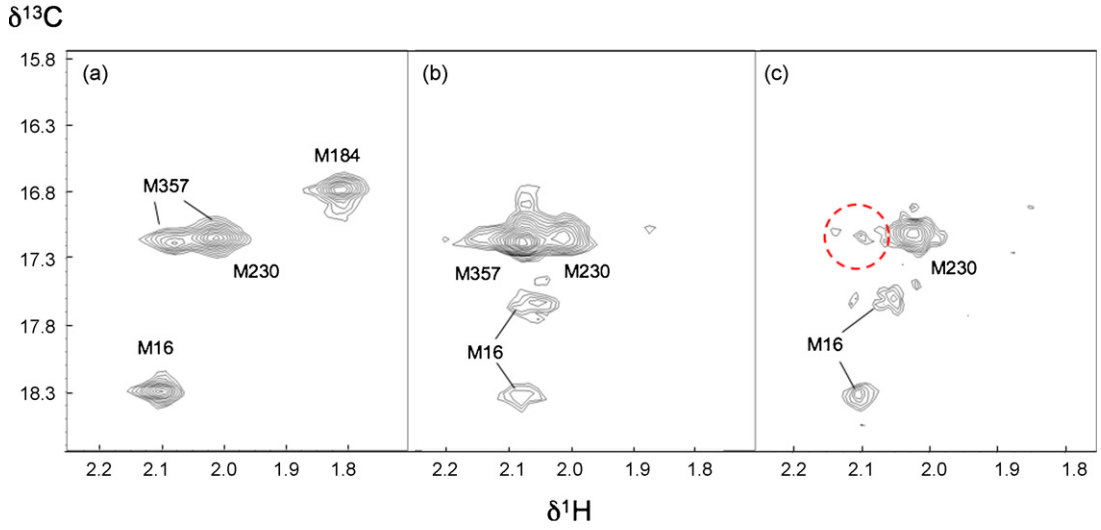

Fig. 2. ^{1}H–^{13}C HSQC spectra of (a) 57 μM [methyl-^{13}C]methionine$_{66}$ RT, (b) 50 μM [methyl-^{13}C]methionine$_{51}$ RT, and (c) 39 μM [methyl-^{13}C]methionine$_{51}$ M357L$_{51}$ RT. The spectrum obtained for the M357L$_{51}$ mutant shown in (c) establishes that the M230 resonance has a similar shift in both subunits. All samples were exchanged into the NMR buffer: 10 mM Tris–HCl-d11, pD 7.6, 200 mM KCl, 1.5 mM sodium azide, 4 mM $MgCl_2$, and 100 μM DSS as an internal chemical shift standard, in D_2O. Spectra were obtained at 25 °C.

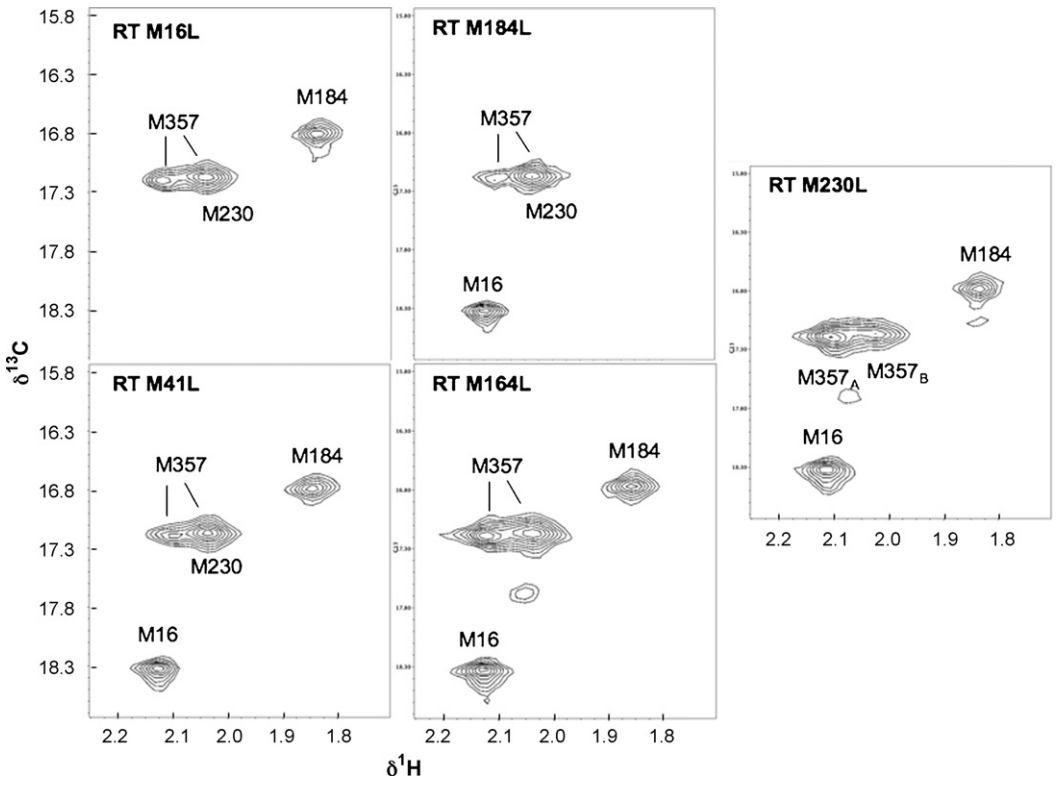

Fig. 3. Site-directed M → L mutants of the p66 subunit of the heterodimer. The $^{1}H–^{13}C$ HSQC spectra of [methyl-^{13}C]methionine$_{66}$ RT containing five site-directed mutants in the p66 subunit are shown. Mutations of M41 and M164 did not produce significant spectral perturbations, consistent with the conclusion that the corresponding resonances are severely broadened. The M230L$_{66}$ mutation does not eliminate the observed resonance intensity due to the appearance of a second M357 resonance with nearly identical shifts.

p66 subunit shown in Fig. 3. Four of the six methionine residues in this subunit give rise to readily observed resonances, while the two residues that are more completely buried with low solvent accessibility, M41 and M164, are not readily observed. Although the use of perdeuteration in combination with the HMQC "TROSY" experiment (Tugarinov et al., 2003) produced modest improvements in resonance intensity, this approach still did not permit unequivocal observation of the two missing resonances (data not shown), perhaps due to the presence of α, β, and γ protons on the [methyl-^{13}C]methionine which compromise the isolation of the $^{13}CH_3$ spin system that is the basis for the TROSY effect (Tugarinov et al., 2003).

Assignment of the M357 resonance proved to be particularly challenging. This appears to result from the conformational flexibility of the M357 loop, as well as the fact that in the p66 subunit, this residue is positioned fairly close to the subunit interface, introducing the possibility that its shift will be dependent on dimer formation. Site-directed substitution of M230 did not completely eliminate the intensity of the resonance at (2.01, 17.14) assigned to M230 so that M357$_{66}$ resonates at two positions (Fig. 4). As expected, the M230 resonance and both M357 resonances were not observed in the double M230L, M357L mutant (data not shown). The complex behavior of M357 is discussed further in the following sections.

The $^{1}H–^{13}C$ HSQC spectrum of [methyl-^{13}C]methionine$_{51}$ RT is somewhat similar to that obtained for the labeled p66 subunit (Fig. 2b) with a number of important differences. In particular, the M184 resonance is no longer clearly resolved, and the resonance intensity of M357 is dramatically increased relative to that of the other methionine peaks. The absence of a resolved M184 resonance indicates that, as with residues M41 and M164, M184 becomes buried in the interior of the protein, resulting in a significantly shorter T_2, and possibly a significant exchange broadening contribution. The increased intensity of M357$_{51}$ indicates a significantly greater internal mobility for this residue in the p51 subunit, compared with the p66 subunit. Perhaps the most surprising result of the study was the observation that, despite apparently different structural environments, residue M230 exhibits similar shifts in both the p66 and p51 subunits. Due to overlap problems of the M357 and M230 resonances, this assignment was verified by examination of the heterodimer formed from p66 and [methyl-^{13}C]methionine M357L$_{51}$ (Fig. 2c). Finally, site-directed mutants demonstrate that in both subunits, M16 gives rise to two resonances at $\delta^{1}H,\delta^{13}C$ = (2.12, 18.35) and (2.07, 17.66). For the P66 subunit, the intensity of the (2.12, 18.35) resonance is much greater, while the two M16 resonances are approximately equal in the p51 subunit.

Further interpretation of the NMR data can be made based on comparisons of experimental NMR signal intensity and shift data with model-based predictions utilizing crystallographic models for the apo enzyme that are summarized in Tables 1 and 2. In large proteins, solvent accessibility is expected to be directly correlated with signal intensity. This correlation has been observed in other large systems such as UvrB (Dellavecchia et al., 2007), and is supported by theoretical studies indicating that packing density is strongly correlated with order parameter (Ming and Bruschweiler, 2004). Solvent accessibility and ^{1}H shifts were determined from four reported crystal structures of uncomplexed RT, pdb codes 1DLO (Hsiou et al., 1996), 1HMV (Rodgers et al., 1995), 1RTJ (Esnouf et al., 1995), and 3DLK (Bauman et al., 2008). We also utilized the structure reported for a truncated construct that includes the palm and fingers subdomains or RT216, 1HAR (Unge et al., 1994). Three of the four structures for the full RT enzyme have a closed thumb conformation for p66 in which the thumb subdomain is positioned closer to the fingers subdomain, while the 1RTJ structure has an open thumb conformation, more similar to that of the RT·RNA·DNA complex (pdb code: 1HYS, Sarafianos et al., 2001) (Fig. 1a and b).

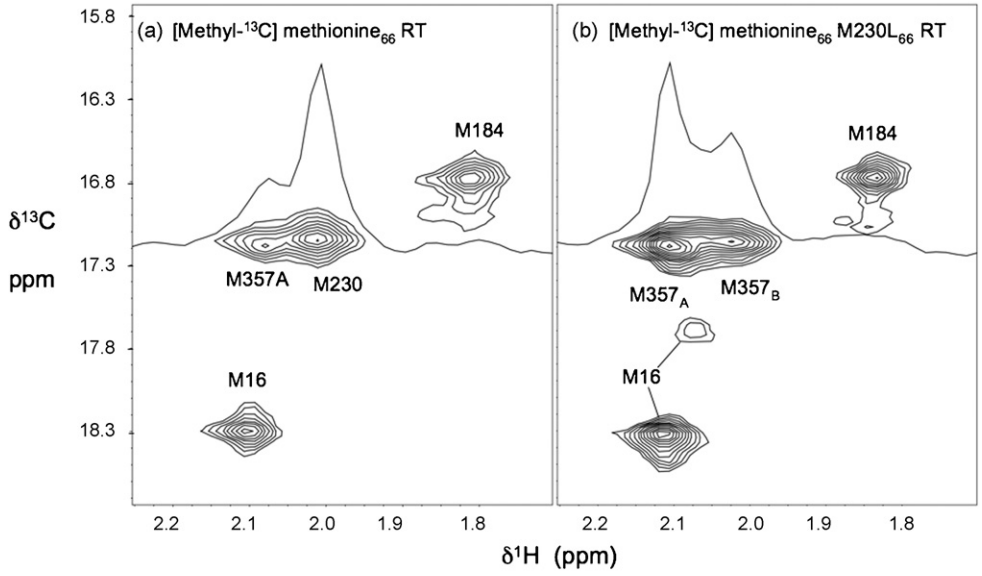

Fig. 4. Superposition of two resonances at δ^1H,^{13}C = (2.03, 17.17). ^{1}H–^{13}C HSQC of (a) [methyl-^{13}C]methionine$_{66}$ RT, and (b) [methyl-^{13}C]methionine$_{66}$ M230L$_{66}$ RT showing the 1D ^{1}H slice at δ^{13}C = 16.9 ppm. This observation, in combination with other studies, indicates that M357$_{66}$ produces two distinct resonances, one of which is degenerate with that of M230$_{66}$.

These conformational differences among the apo RT structures are related to the different space groups of the RT crystals corresponding to different crystallization conditions (Table 1). The open 1RTJ structure was obtained by crystallization of RT in the presence of 1-[(2-hydroxyethoxy)methyl]-6-(phenylthio)thymine (HEPT), a weak NNRTI, which was subsequently soaked out of the crystal (Esnouf et al., 1995). We note here that the open/closed orientation of the thumb subdomain illustrated in Fig. 1a and b is not to be confused with the major conformational rearrangement of the first 440 residues of RT, which can adopt a more globular, p51-like conformation or an "extended", p66-like conformation. As can be seen both from an examination of the structures and from the data summarized in Table 1, there is a dramatic reduction in the solvent exposure of M184 in the p51 subunit, as the active site becomes largely solvent inaccessible. The fractional solvent exposure of M184 averaged among the four reported crystal structures of uncomplexed RT is 0.60 for p66 and 0.13 in p51 (Table 1). Thus, the loss of resonance intensity is readily explained in terms of the greater dipolar relaxation contributions to the buried residue.

In addition to interpreting the intensity of the resonances in terms of solvent exposure, we also utilized structure-based ^{1}H shift predictions, summarized in Table 2 (Neal et al., 2003) The M184$_{66}$ resonance exhibits an upfield ^{1}Hε shift of 1.84 ppm, which results primarily from its proximity to Y183$_{66}$. The ^{1}H shift values predicted by SHIFTX (Neal et al., 2003) from the crystal structures (Table 2) for M184$_{66}$ range from 1.89 ppm (3DLK) to 2.21 (1RTJ), with the variation resulting primarily from variability in the relative position of Y183$_{66}$ and M184$_{66}$ (Fig. 1c). In silico rotation of the Y183$_{66}$ phenol sidechain can vary the predicted shift up or downfield, dependent on its orientation relative to the M183$_{66}$ methyl group. The predicted M184$_{66}$ ^{1}H shift for structure 1RTJ shows the poorest agreement with experiment, and has the methion-

Table 1
Comparison of methionine methyl resonance intensities with crystal structure-based residue solvent exposure.

Residue	NMR resonance intensity[a]	Crystal structures				
		1DLO apo	1HMV apo	3DLK apo	1RTJ apo	1HAR Fingers–palm
Space group		C2 (1 2 1)	C2 (1 2 1)	C2 (1 2 1)	$P2_12_12_1$	$P4_3$
Resolution		2.70	3.20	1.85	2.35	2.20
I: p66 subunit						
M16	1.0	0.46	0.41	0.43	0.45	0.33
M41	–	0.04	0.16	0.10	0.13	0.10
M164	–	0.0	0	0.02	0	0.01
M184	0.87	0.38	0.71	0.62	0.67	0.59
M230	1.16 – 0.34 = 0.82[b]	0.01	0.10	0.09	0.50	
M357	0.55 + 0.34 = 0.89[b]	[c]	0.26	0.72	0.92	
II: p51 subunit						
M16	1.0	0.44	0.47	0.37	0.45	
M41	–	0.08	0.11	0.05	0.13	
M164	–	0.02	0.03	0.05	0.01	
M184	0	0.09	0.18	0.11	0.15	
M230	1.39	[d]	[d]	0.11	[d]	
M357	4.1	[c]	[c]	0.58	0.53	

[a] Resonance intensities are normalized relative to the total intensity of both M16 resonances.
[b] Intensities of the M230 and M357 resonances are corrected for the overlap of M230$_{66}$ with M357$_{66}$ (see Fig. 4).
[c] The M357 loop is disordered in both subunits of 1DLO, and in the p51 subunit of 1HMV.
[d] Segments containing M230 are disordered in the p51 subunit of 1DLO, 1HMV, and 1RTJ. Structure 3DLK contains M230, however residues 214-225 are disordered.

Table 2
NMR shift values and structure-based methionine methyl proton shift predictions (SHIFTX).

Residue		Crystal structures				
		1DLO	1HMV	3DLK	1RTJ	1HAR
Ligand		apo	apo	apo		
Resolution		2.70	3.20	1.85	2.35	2.20
I: p66 subunit						
	NMR data					
Residue	δ^1H					
M16	2.10	2.11	2.13	2.12	2.11	2.07
M41	–	2.27	2.09	2.78	1.76	1.70
M164	–	2.06	2.11	2.11	1.86	1.94
M184	1.81	2.03	1.99	1.89	2.21	2.03
M230	2.01	0.90	−0.97	1.55	2.07	
M357	2.08	–	2.14	2.16	2.13	
II: p51						
M16	2.10	2.10	2.08	2.11	2.13	
M41	–	1.95	2.00	1.99	2.06	
M164	–	2.09	2.13	2.14	2.13	
M184	1.81	2.22	2.40	2.15	1.78	
M230	2.02	–	–	1.75	–	
M357	2.11	–	–	2.13	2.04	

SHIFTX calculations utilized the web-based site, http://redpoll.pharmacy.ualberta.ca/shiftx, described by Neal et al. (2003).

ine sidechain oriented at the edge of Y183 with the methyl group pointing away from the phenyl ring. The observed interaction of $M184_{66}$ and $Y183_{66}$ is consistent with the substantial literature on methionine–phenylalanine interactions (Klingler and Brutlag, 1994; Stapley et al., 1995).

In contrast with the results discussed above for $M184_{66}$, the predicted shift and intensity parameters for $M230_{66}$ show substantially poorer agreement with the observed values. $M230_{66}$ is located at the end of a β-hairpin that forms part of the polymerase primer binding site of RT (Fig. 1c) (Ghosh et al., 1996; Powell et al., 1997; Sarafianos et al., 2001). The position of the β9–β10 primer grip hairpin differs markedly among these structures. Although the $M230_{66}$ resonance is fairly intense, three of the four structures predict limited solvent exposure, which as discussed above for M41 and M164, is expected to correspond to very weak resonance intensity. In contrast, structure 1RTJ corresponds to a fractional solvent accessibility of 0.50 for $M230_{66}$, consistent with a more intense resonance. The three structures in which $M230_{66}$ has little solvent accessibility also led to SHIFTX predictions of significant upfield ^{1}Hε shifts, averaging 0.5 ppm, in contrast with the observed value of 2.04 ppm (Table 2). Thus, there appear to be significant differences between the environment of $M230_{66}$ in solution as determined from the NMR studies, and crystal structure-based predictions of shift and intensity using structures 1DLO, 1HMV, and 3DLK. Alternatively, the 1RTJ-based ^{1}Hε shift prediction of 2.07 ppm and the solvent exposure-based intensity predictions are more consistent with the observed resonance behavior. In the p51 subunit, M230-containing peptide segments of length 12–23 residues are disordered in three of the four structures summarized in Table 1. This behavior is consistent with the observed shift and intensity of the $M230_{51}$ resonance in [methyl-^{13}C]methionine$_{51}$ RT. Alternatively, the behavior of the $M230_{51}$ resonance is inconsistent with the parameters predicted on the basis of structure 3DLK, and also is inconsistent with a model that assumes rapid or intermediate exchange between the ordered structure observed in 3DLK and the disordered structures of the other crystal structures.

Plots of methyl resonance intensity vs. the fractional solvent exposure averaged among the four structures generally show the expected correlation for larger proteins (Fig. 5). The intensities of the $M357_{66}$ and $M230_{66}$ resonances were corrected for the overlap illustrated in Fig. 4. Consistent with the above discussion, a significant improvement in the predicted intensity for the $M230_{66}$ resonance is obtained using the solvent accessibility calculated for structure 1RTJ, rather than the average value. Due to its location near the subunit interface (Fig. 6), the actual solvent accessibility of $M357_{66}$ will probably be somewhat lower than the calculated value, depending on the particular structure used for the calculation.

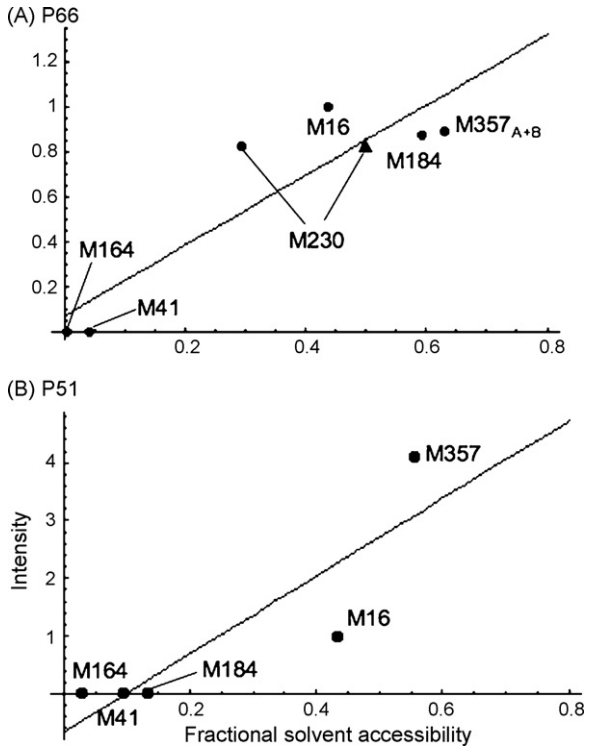

Fig. 5. Plots of relative intensity vs. solvent accessibility for P66 (a) and P51 (b) subunits of RT. NMR intensities for each subunit are normalized relative to the value for M16. For the p51 subunit, normalization was based on the sum of the intensities of the two M16 resonances. Solvent accessibilities for each of the apo RT structures summarized in Table 1 were calculated using the program VADAR (Willard et al., 2003), and the average values were used for the plot. The values for $M357_{66}$ and $M230_{66}$ were calculated by dividing the overlapping resonance into two components based on the data for the M230L mutant shown in Fig. 4. A data point is also included for $M230_{66}$ using only the solvent accessibility for the 1RTJ structure (filled triangle).

3.1. Complex behavior of the M357 loop

In both the p66 and p51 subunits, M357 lies on a loop connecting β-strand 18 with α-helix K (Wang et al., 1994). This loop was disordered in three of the four p51 subunits and one of the p66 subunits of the apo structures analyzed in Tables 1 and 2. According to the analysis given above, the shift of the $M357_{66}$ resonance in the p66 subunit is perturbed slightly due to its proximity to the dimer interface (Fig. 6). Studies of [methyl-^{13}C]methionine$_{66}$ $M230L_{66}$ RT revealed that although most of the resonance at the initial M230 position was eliminated, a significant residual peak at this "B" position remained (Fig. 4). One interpretation of this behavior consistent with the intensities observed for the M357 resonances is that in the p51 subunit, the M357 loop undergoes rapid conformational averaging on a ns time scale, while in the p66 subunit, there is a slower equilibrium involving at least two relatively stable conformations. This difference in dynamic behavior presumably results as a consequence of the proximity of $M357_{66}$ to the dimer interface. Consistent with the dynamic conclusions summarized above, analysis of the Cα B-factor values for structure 3DLK indicates that the average value for residues 355–361 jumps to 88 relative to an

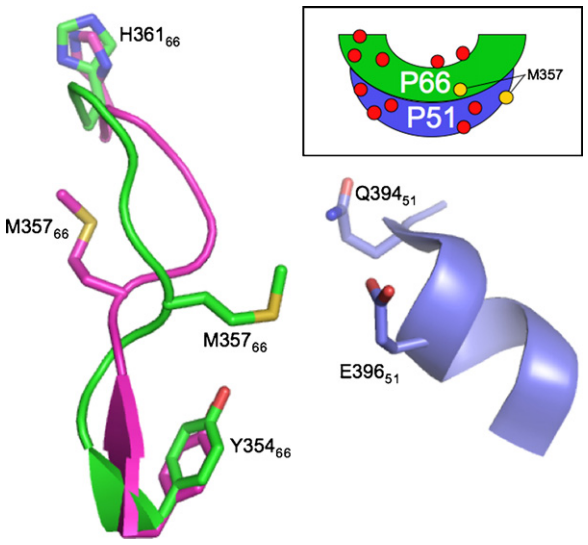

Fig. 6. Environment of M357. (a) The structure of the region near M357$_{66}$ is based on crystal structure 3DLK (Bauman et al., 2008), with p66 residues shown in green and p51 in blue. In order to illustrate the conformational heterogeneity of this loop, we also have included an overlay of the segment from residues Y354$_{66}$-H361$_{66}$ derived from structure 1HMV (magenta). In this structure the M357$_{66}$ loop adopts an altered conformation, characterized by flipping of the R356-M357-R358 sidechains. For clarity, only the sidechains for Y354$_{66}$, M357$_{66}$, H361$_{66}$, Q394$_{51}$ and E396$_{51}$ are shown. The inset shows a schematic representation of the positions of the M357 residues relative to the overall structure of the heterodimer. (For interpretation of the references to color in this figure legend, the reader is referred to the web version of the article.).

average of 36 for the entire p51 connection subdomain. A qualitatively similar but much smaller jump–from 34 to 56, occurs for the corresponding residues in the p66 subunit.

Crystal structure data suggest some possibilities for the identity of the conformational change influencing the M357$_{66}$ shift. In structure 1HMV, the M357 loop adopts an alternate conformation in which the orientation of the R356-M357-R358 sidehchains is approximately reversed relative to the positions in 3DLK (Fig. 6). Although the resolution of the 1HMV structure is 3.2 Å, similar conformations are evident in some more highly resolved structures of RT drug complexes, such as 3DYA (Sweeney et al., 2008). In summary, the M357 loop of the p51 subunit undergoes rapid segmental motion leading to a very intense resonance, while the M357 loop on the p66 subunit appears to be sensitive to dimer formation and undergoes slower exchange between at least two different conformational states.

3.2. Effect of nevirapine

Non-nucleoside reverse transcriptase inhibitors (NNRTI) such as nevirapine play an important role in the treatment of HIV; however, fundamental questions about the mechanistic basis for their inhibition remain unanswered. Biochemical evidence indicates that NNRTIs do not affect the ability of RT to form a ternary complex with nucleic acid and nucleoside triphosphate, but specifically inhibit the chemical step of nucleotide incorporation into the primer strand (Spence et al., 1995; Rittinger et al., 1995), consistent with observed distortions of residues in the polymerase active site. These inhibitors bind in the vicinity of the two active site β-hairpins that contain the M184 and M230 residues. The HSQC spectra of [methyl-^{13}C]methionine$_{66}$ RT and [methyl-^{13}C]methionine$_{51}$ RT indicate that only methionine resonances in the p66 subunit are sensitive to the addition of nevirapine, with M184$_{66}$, M230$_{66}$ exhibiting significant shifts (Fig. 7). Venezia et al. (2006) suggest that a conformational change in the I135-P140 segment of the p51 subunit accompanies binding of the NNRTI efavirenz. This region is near the active site, but far from the labeled methionine residues in p51, so that although a similar conformational change might also occur in response to nevirapine, it would not be observed in the present study.

Addition of nevirapine resulted in a downfield ^{1}H shift of 0.10 ppm for the M184$_{66}$ resonance, which could be rationalized on the basis of a small change in the relative orientation of M184$_{66}$ and Y183$_{66}$, while the M230$_{66}$ resonance exhibits larger ^{1}H and ^{13}C shift changes: $\Delta^{1}H,^{13}C = (-0.21, -1.19)$ ppm. In addition, resonance M357$_{B}$ also appears to exhibit a small shift in response to nevirapine addition (Fig. 7a). The crystal structure of the nevirapine complex (pdb code: 1VRT, Ren et al., 1995) indicates very significant changes in the relative position of the primer grip, with the M184$_{66}$ residue being brought into close contact with Y183$_{66}$. Indeed, the distance and relative orientation of these two residues

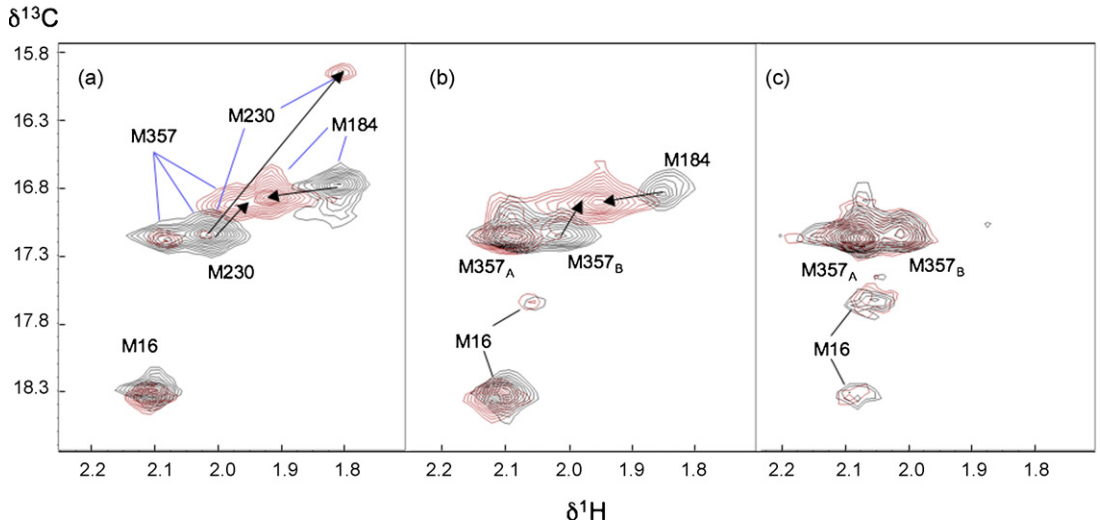

Fig. 7. Effect of nevirapine on RT. (a) ^{1}H–^{13}C HSQC spectra of uncomplexed [methyl-^{13}C]methionine$_{66}$ RT (57 μM) in the absence (black) and presence (red) of 250 μM nevirapine; (b) ^{1}H–^{13}C HSQC spectra of uncomplexed [methyl-^{13}C]methionine$_{66}$ M230L$_{66}$ RT (60 μM) in the absence (black) and presence (red) of 100 μM nevirapine; (c) ^{1}H–^{13}C HSQC spectra of uncomplexed [methyl-^{13}C]methionine$_{51}$ RT (50 μM) in the absence (black) and presence (red) of 200 μM nevirapine. The arrows indicate resonance shifts in response to the nevirapine. NMR parameters and buffer as in Fig. 2. (For interpretation of the references to color in this figure legend, the reader is referred to the web version of the article.).

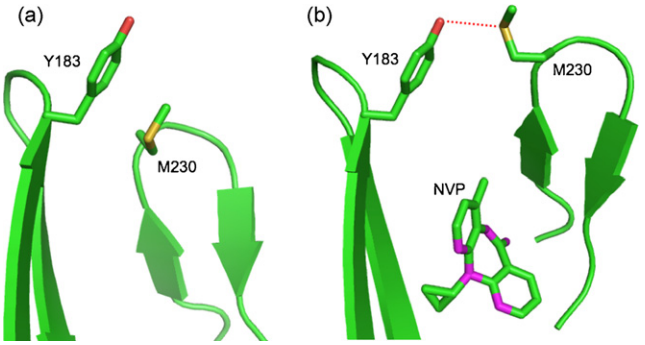

Fig. 8. Effect of nevirapine on the RT active site. The structure of the two methionine-containing β-hairpins corresponding to the active site YMDD motif (β9–β10 hairpin), and to the primer grip (β12–β13 hairpin) in the absence (a) and presence (b) of nevirapine (1VRT). The proximity of M230 S to Y183 OH is consistent with an OH···S hydrogen bond interaction in the nevirapine complex.

is consistent with a hydrogen bonding interaction between the hydroxyl group of $Y183_{66}$ and the $M230_{66}$ sulfur atom (Gregoret et al., 1991) (Fig. 8). Interestingly, similar structural changes consistent with a $Y183_{66}$-$M230_{66}$ hydrogen bond can also be observed in RT-efavirenz complexes (e.g. pdb structures 1FK9, 1IKW). Based on the reported crystal structures, the $^{1}H\varepsilon$ shifts for $M184_{66}$ and $M230_{66}$ do not result from direct interactions with the nevirapine, but are dominated by indirect effects resulting from perturbation of the relative orientations of the nearby $Y183_{66}$ and $W229_{66}$ residues. Structure-based ^{1}H shift predictions are qualitatively consistent with some of these shift changes, but do not provide a reliable quantitative basis for interpretation of the small shifts due to the limited resolution of these structures and the extreme sensitivity of the shifts to small changes in orientation. Nevertheless, some structural features can be critically evaluated. For example, structure 1LWE, which corresponds to the nevirapine complex of the M41L, T215Y doubly mutated RT, has a W229 conformation that differs from that of the other nevirapine complexes, and the SHIFTX program predicts a $^{1}H\varepsilon$ shift of 0.02 ppm for M230, in sharp contrast with the observed value of 1.81 ppm. Hence, the corresponding W229 rotamer conformation is not significantly populated in solution.

In contrast with the ^{1}H data, the large nevirapine-induced ^{13}C shift of −1.19 ppm for $M230_{66}$ probably arises from a change in the distribution of methionine $\chi 3$ values. Recent statistical studies indicated that *gauche* orientations for methionine $\chi 3$ were correlated with an upfield ^{13}C shift of ∼−1.78 ppm relative to the *trans* conformers (London et al., 2008). Investigation of several nevirapine-containing RT structures including 1VRT, 1LW0, 1LWC, 1JLB, 1JLF (Ren et al., 1995; Ren et al., 2001; Chamberlain et al., 2002) show that in the nevirapine complex, the interaction between $Y183_{66}$ and $M230_{66}$ interferes with the *trans* conformation and may further stabilize the *gauche* conformation of $M230_{66}$ $\chi 3$ as a consequence of hydrogen bonding between $Y183_{66}$ OH and $M230_{66}$ S. There is no analogous constraint in the apo structures, particularly for the open thumb conformation observed in 1RTJ, and no structure of the apo enzyme is consistent with a similar hydrogen bonding interaction. Hence, we conclude that the fractional *trans* probability for $M230_{66}$ $\chi 3$ is reduced in the nevirapine complex, leading to the upfield ^{13}C shift.

The small shift of the $M357_{B}$ resonance in the p66 subunit (Fig. 7a and b) may result from structural changes at the subunit interface, or from the transition from a more closed to an open conformation of the p66 subunit, similar to that illustrated in the 1RTJ structure (Fig. 1b). Since nevirapine increases the RT dimer formation constant, it would not be surprising for it to influence the shift of $M357_{66}$ due to its location near the interface. In contrast, the $M357_{A}$ component at (2.08, 17.16), which has the same shift as $M357_{51}$, is not significantly perturbed by the nevirapine.

4. Discussion

Due to the importance of HIV reverse transcriptase as a drug target, it has been studied using a broad range of biophysical techniques. However, the size and complexity of the enzyme make it a challenging target for NMR studies, and to the best of our knowledge, no direct NMR studies have been reported, although nucleotide binding has been studied using the transferred NOE approach (Painter et al., 1993). The strategic location of methionine in both the active site YMDD motif on the β9–β10 hairpin as well as on the β12–β13 primer grip, along with the high mobility of the residue which results in significant line narrowing, makes the use of [methyl-^{13}C]methionine an ideal label for NMR investigation of HIV reverse transcriptase. Surprisingly, the behavior of the methyl resonances for the two active site methionine residues is dramatically different. The M184 resonance characteristics are strongly dependent on which subunit is labeled. The $M184_{66}$ resonance exhibits characteristic shift and intensity parameters that are at least qualitatively consistent with crystal structure-based predictions, while in the p51 subunit, the resonance is not readily detected, consistent with expectations for a residue with low solvent accessibility. These features are generally consistent with expectations derived from crystal structure data.

In contrast, the M230 resonances from both subunits produce resonances that are similar in both shift and intensity. The behavior of the M230 resonances is consistent with residues that have substantial solvent accessibility and motional freedom, although it cannot be ruled out that the observed resonances in either subunit may be in slow exchange with additional conformational state(s) that are not readily observed by NMR due to their relaxation characteristics. More specifically, if the interconversion of the closed and open enzyme conformations illustrated by the crystal structures in Fig. 1 is sufficiently slow on the chemical shift time scale, the NMR observation might be selective for the more flexible M230 environment characterizing the open conformation. The shift parameters are typical for solvent-exposed methionine residues that are influenced primarily by local, sequence-dependent interactions, rather than by constrained long-range interactions with aromatic residues. For the p51 subunit, segments containing M230 are disordered in three of the apo structures considered, while in structure 3DLK, $M230_{51}$ is observed, although an adjacent segment from residues 214–225 is not. The NMR data indicates that in solution, the behavior of $M230_{51}$ is more consistent with expectations based on the disordered segment. We emphasize, however, that in contrast to M357, the M230 resonance does not exhibit the high intensity characteristic of a disordered segment with large amplitude fluctuations on the ns time scale. Instead, the M230 resonance characteristics are consistent with a residue that may be involved in some degree of conformational exchange occurring on the μs time scale, characterized by a more limited range of motion.

As discussed in detail in the previous section, the $M230_{66}$ resonance parameters are generally not consistent with the closed structures of apo RT observed in various crystal studies. In these structures, $M230_{66}$ has considerably lower solvent accessibility, as well as interactions with remote residues that are predicted to produce significant broadening and shift perturbations. The NMR parameters for $M230_{66}$ are, however, consistent with the highly unusual ability of the region of RT near this residue to interact with NNRTI. This type of interaction, resulting in formation of a binding pocket that is not observed in the apo structure, requires substantial conformational plasticity and is thus consistent with the observed resonance characteristics that correspond to a solvent accessible, disordered environment. Interestingly, most of the

structures reported for apo RT adopt an inactive conformation characterized by a closed fingers–thumb orientation that precludes DNA/RNA binding, and the pivot points for rigid-body motion of the fingers and thumb subdomains are located near the NNRTI binding pocket (Ivetac and Mccammon, 2009). Thus, the apparent inconsistency with the behavior of the observed $M230_{66}$ resonance is not that surprising. Additionally, there are substantial structural differences even among the three closed structures, in the region near $M230_{66}$, and even the $M230_{66}$ $\chi 1$ angle varies significantly. This variability is the basis for the large variations in the SHIFTX-based ^{1}H shift predictions for $M230_{66}$ (Table 2). Although the data for the $M230_{66}$ resonance are more consistent with structure 1RTJ, with an open fingers–thumb conformation, the observed parameters might equally correspond to an ensemble of structures, with many having a relatively unconstrained M230 residue. ESR studies of spin-labeled RT have found that at 25° C, the enzyme adopts the closed conformation with ~84% probability (interpolated from the reported values, Kensch et al., 2000), so the remaining 16% in the open conformation may be sufficient to explain the NMR observations. More probably, the structural coupling between the active site conformation and the fingers–thumb orientation is imperfect, allowing for greater flexibility of the active site residues.

An alternate interpretation for the similarities between the $M230_{66}$ and $M230_{51}$ resonances is that partial proteolytic processing of the p66 subunit of RT occurs in the *E. coli*, as has been observed previously (Maier et al., 1999). As a result, ^{13}C labeling in the p66 subunit could be contaminated with some label in the p51 subunit. In addition to the coincident $M230_{66}$ and $M230_{51}$ shifts, this process could also explain the observation of two $M357_{66}$ resonances. Despite this possibility, chromatographic analysis showed no significant presence of a p51 peak in the p66 preparation. Consistent with the above conclusion, MALDI-TOF mass spectrometric analysis of methionine-containing tryptic peptides from p51 showed no measurable difference of the isotope composition from natural abundance (data not shown), indicating essentially no measurable proteolysis of p66 to p51 under the conditions of our study.

The observation of two resonances arising from M16, located on the protein surface, was also unanticipated. In all reported structures, the K13-P14-G15-M16 residues form a Type II β-turn, and it is possible that the observed resonances may result from significant *cis*/*trans* isomerism of the K13–P14 bond. There are many precedents for observation of multiple resonances near conformationally heterogeneous X-Pro bonds (Hinck et al., 1993; Pitcher et al., 2003). The possibility that the observed heterogeneity is a consequence of variable processing of the N-terminal methionine and/or additional N-terminal residues is extremely unlikely, since M16 is ~30 Å from the N-terminus. Additionally, Thimmig and McHenry (1993) have demonstrated >95% cleavage of the N-terminal Met-Pro bond of HIV RT expressed in *E. coli*, consistent with our failure to observe an N-terminal methionine methyl resonance. Also surprising is the variability in the ratio of the $\delta^{13}C = 17.7/\delta^{13}C = 18.3$ ppm M16 resonances; in the P66 subunit the intensity of the 18.3 ppm resonance is much greater than that of the 17.7 ppm resonance, while in p51, the intensities of the two components have similar intensity. We are aware of no significant data indicating greater conformational heterogeneity for the fingers subdomain of p51, and examination of the crystal structures provides no insight into the basis for these differences, so that at the present time this observation requires further investigation.

The present study extends the conclusions obtained previously on methionine labeled UvrB (MW 75 kD), indicating that in these large systems, solvent accessibility becomes a dominant factor in determining the observability of the methionine methyl resonances (Dellavecchia et al., 2007). For RT, the resonances arising from the buried M41 and M164 residues could not be unequivocally assigned, even after perdeuteration of the protein. Although qualitatively similar effects can be observed for small and moderately sized proteins such as Pol β (40 kD) in which buried methionine residues can readily be observed (Bose-Basu et al., 2004), transverse relaxation becomes much more significant for large systems such as UvrB and RT. Alternatively, deviations from the predicted solvent–accessibility–intensity relationship generally indicate important conformational exchange contributions or a lack of applicability of the structural model to the solution behavior, as is apparently the case for M230 of RT.

In addition to the pronounced effects of nevirapine on the active site methionine residues, there is a small perturbation of the $M357_{B}$ resonance so that it partially overlaps the shifted $M184_{66}$ resonance. Based on the position of $M357_{66}$ near the dimer interface and the well documented effects of NNTRI on dimerization behavior (e.g., Venezia et al., 2006), the observed effect is probably not surprising. In addition, the stabilization of an open conformation of p66 places the thumb subdomain much closer to M357, so that this conformational effect could also be related to the observed shift perturbation. Ongoing studies with spin-labeled RT should help to clarify these effects.

Acknowledgement

This research was supported by Research Project number Z01-ES050147 to REL in the Intramural Research Program of the National Institutes of Health.

References

Autran, B., Carcelain, G., Li, T.S., Blanc, C., Mathez, D., Tubiana, R., Katlama, C., Debre, P., Leibowitch, J., 1997. Positive effects of combined antiretroviral therapy on CD4(+) T cell homeostasis and function in advanced HIV disease. Science 277, 112–116.

Bauman, J.D., Das, K., Ho, W.C., Baweja, M., Himmel, D.M., Clark, A.D., Oren, D.A., Boyer, P.L., Hughes, S.H., Shatkin, A.J., Arnold, E., 2008. Crystal engineering of HIV-1 reverse transcriptase for structure-based drug design. Nucleic Acids Res. 36, 5083–5092.

Bose-Basu, B., DeRose, E.F., Kirby, T.W., Mueller, G.A., Beard, W.A., Wilson, S.H., London, R.E., 2004. Dynamic characterization of a DNA repair enzyme: NMR studies of [methyl-C-13]methionine-labeled DNA polymerase beta. Biochemistry 43, 8911–8922.

Chamberlain, P.P., Ren, J., Nichols, C.E., Douglas, L., Lennerstrand, J., Larder, B.A., Stuart, D.I., Stammers, D.K., 2002. Crystal structures of zidovudine- or lamivudine-resistant human immunodeficiency virus type 1 reverse transcriptases containing mutations at codons 41, 184, and 215. J. Virol. 76, 10015–10019.

Das, K., Sarafianos, S.G., Clark, A.D., Boyer, P.L., Hughes, S.H., Arnold, E., 2007. Crystal structures of clinically relevant Lys103Asn/Tyr181Cys double mutant HIV-1 reverse transcriptase in complexes with ATP and non-nucleoside inhibitor HBY 097. J. Mol. Biol. 365, 77–89.

Delaglio, F., Grzesiek, S., Vuister, G.W., Zhu, G., Pfeifer, J., Bax, A., 1995. NMRPipe: a multidimensional spectral processing system based on UNIX pipes. J. Biomol. NMR 6, 277–293.

Dellavecchia, M.J., Merrittt, W.K., Peng, Y., Kirby, T.W., Derose, E.F., Mueller, G.A., Van Houten, B., London, R.E., 2007. NMR analysis of [methyl-C-13]methionine UvrB from Bacillus caldotenax reveals UvrB-domain 4 heterodimer formation in solution. J. Mol. Biol. 373, 282–295.

Ding, J., Das, K., Hsiou, Y., Sarafianos, S.G., Clark Jr., A.D., Jacobo-Molina, A., Tantillo, C., Hughes, S.H., Arnold, E., 1998. Structure and functional implications of the polymerase active site region in a complex of HIV-1 RT with a double-stranded DNA template-primer and an antibody Fab fragment at 2.8 A resolution. J. Mol. Biol. 284, 1095–1111.

Esnouf, R., Ren, J., Ross, C., Jones, Y., Stammers, D., Stuart, D., 1995. Mechanism of inhibition of HIV-1 reverse transcriptase by non-nucleoside inhibitors. Nat. Struct. Biol. 2, 303–308.

Ghosh, M., Jacques, P.S., Rodgers, D.W., Ottman, M., Darlix, J.L., Le Grice, S.F., 1996. Alterations to the primer grip of p66 HIV-1 reverse transcriptase and their consequences for template-primer utilization. Biochemistry 35, 8553–8562.

Gregoret, L.M., Rader, S.D., Fletterick, R.J., Cohen, F.E., 1991. Hydrogen bonds involving sulfur atoms in proteins. Proteins 9, 99–107.

Gutierrez-Rivas, M., Menendez-Arias, L., 2001. A mutation in the primer grip region of HIV-1 reverse transcriptase that confers reduced fidelity of DNA synthesis. Nucleic Acids Res. 29, 4963–4972.

Hinck, A.P., Eberhardt, E.S., Markley, J.L., 1993. NMR strategy for determining Xaa-Pro peptide bond configurations in proteins: mutants of staphylococcal nuclease with altered configuration at proline-117. Biochemistry 32, 11810–11818.

Hou, E.W., Prasad, R., Beard, W.A., Wilson, S.H., 2004. High-level expression and purification of untagged and histidine-tagged HIV-1 reverse transcriptase. Protein Expr. Purif. 34, 75–86.

Hsiou, Y., Ding, J., Das, K., Clark, A.D., Hughes, S.H., Arnold, E., 1996. Structure of unliganded HIV-1 reverse transcriptase at 2.7 angstrom resolution: Implications of conformational changes for polymerization and inhibition mechanisms. Structure 4, 853–860.

Ivetac, A., Mccammon, J.A., 2009. Elucidating the inhibition mechanism of HIV-1 non-nucleoside reverse transcriptase inhibitors through multicopy molecular dynamics simulations. J. Mol. Biol. 388, 644–658.

Johnson, B.A., Blevins, R.A., 1994. NMR view—a computer-program for the visualization and analysis of NMR Data. J. Biomol. NMR 4, 603–614.

Kensch, O., Restle, T., Wohrl, B.M., Goody, R.S., Steinhoff, H.J., 2000. Temperature-dependent equilibrium between the open and closed conformation of the p66 subunit of HIV-1 reverse transcriptase revealed by site-directed spin labelling. J. Mol. Biol. 301, 1029–1039.

Klingler, T.M., Brutlag, D.L., 1994. Discovering structural correlations in alpha-helices. Protein Sci. 3, 1847–1857.

Kohlstaedt, L.A., Wang, J., Friedman, J.M., Rice, P.A., Steitz, T.A., 1992. Crystal-structure at 3.5 Angstrom resolution of Hiv-1 reverse-transcriptase complexed with an inhibitor. Science 256, 1783–1790.

London, R.E., Wingad, B.D., Mueller, G.A., 2008. Dependence of amino acid side chain 13C shifts on dihedral angle: application to conformational analysis. J. Am. Chem. Soc. 130, 11097–11105.

Maier, G., Dietrich, U., Panhans, B., Schroder, B., Rubsamen-Waigmann, H., Cellai, L., Hermann, T., Heumann, H., 1999. Mixed reconstitution of mutated subunits of HIV-1 reverse transcriptase coexpressed in *Escherichia coli*—two tags tie it up. Eur. J. Biochem. 261, 10–18.

Ming, D., Bruschweiler, R., 2004. Prediction of methyl-side chain dynamics in proteins. J. Biomol. NMR 29, 363–368.

Muchmore, D.C., Mcintosh, L.P., Russell, C.B., Anderson, D.E., Dahlquist, F.W., 1989. Expression and nitrogen-15 labeling of proteins for proton and nitrogen-15 nuclear magnetic resonance. Methods Enzymol. 177, 44–73.

Neal, S., Nip, A.M., Zhang, H., Wishart, D.S., 2003. Rapid and accurate calculation of protein 1H, 13C and 15N chemical shifts. J. Biomol. NMR 26, 215–240.

Painter, G.R., Aulabaugh, A.E., Andrews, C.W., 1993. A comparison of the conformations of the 5'-triphosphates of zidovudine (AZT) and thymidine bound to HIV-1 reverse transcriptase. Biochem. Biophys. Res. Commun. 191, 1166–1171.

Pitcher 3rd, W.H., DeRose, E.F., Mueller, G.A., Howell, E.E., London, R.E., 2003. NMR studies of the interaction of a type II dihydrofolate reductase with pyridine nucleotides reveal unexpected phosphatase and reductase activity. Biochemistry 42, 11150–11160.

Powell, M.D., Ghosh, M., Jacques, P.S., Howard, K.J., Le Grice, S.F., Levin, J.G., 1997. Alanine-scanning mutations in the "primer grip" of p66 HIV-1 reverse transcriptase result in selective loss of RNA priming activity. J. Biol. Chem. 272, 13262–13269.

Ren, J., Esnouf, R., Garman, E., Somers, D., Ross, C., Kirby, I., Keeling, J., Darby, G., Jones, Y., Stuart, D., et al., 1995. High resolution structures of HIV-1 RT from four RT-inhibitor complexes. Nat. Struct. Biol. 2, 293–302.

Ren, J., Nichols, C., Bird, L., Chamberlain, P., Weaver, K., Short, S., Stuart, D.I., Stammers, D.K., 2001. Structural mechanisms of drug resistance for mutations at codons 181 and 188 in HIV-1 reverse transcriptase and the improved resilience of second generation non-nucleoside inhibitors. J. Mol. Biol. 312, 795–805.

Rittinger, K., Divita, G., Goody, R.S., 1995. Human immunodeficiency virus reverse transcriptase substrate-induced conformational changes and the mechanism of inhibition by nonnucleoside inhibitors. Proc. Natl. Acad. Sci. U.S.A. 92, 8046–8049.

Rodgers, D.W., Gamblin, S.J., Harris, B.A., Ray, S., Culp, J.S., Hellmig, B., Woolf, D.J., Debouck, C., Harrison, S.C., 1995. The structure of unliganded reverse transcriptase from the human immunodeficiency virus type 1. Proc. Natl. Acad. Sci. U.S.A. 92, 1222–1226.

Sarafianos, S.G., Das, K., Tantillo, C., Clark Jr., A.D., Ding, J., Whitcomb, J.M., Boyer, P.L., Hughes, S.H., Arnold, E., 2001. Crystal structure of HIV-1 reverse transcriptase in complex with a polypurine tract RNA:DNA. EMBO J. 20, 1449–1461.

Shen, L., Shen, J., Luo, X., Cheng, F., Xu, Y., Chen, K., Arnold, E., Ding, J., Jiang, H., 2003. Steered molecular dynamics simulation on the binding of NNRTI to HIV-1 RT. Biophys. J. 84, 3547–3563.

Spence, R.A., Kati, W.M., Anderson, K.S., Johnson, K.A., 1995. Mechanism of inhibition of HIV-1 reverse transcriptase by nonnucleoside inhibitors. Science 267, 988–993.

Stapley, B.J., Rohl, C.A., Doig, A.J., 1995. Addition of side chain interactions to modified Lifson-Roig helix-coil theory: application to energetics of phenylalanine-methionine interactions. Protein Sci. 4, 2383–2391.

Studier, F.W., 2005. Protein production by auto-induction in high density shaking cultures. Protein Expr. Purif. 41, 207–234.

Sweeney, Z.K., Harris, S.F., Arora, S.F., Javanbakht, H., Li, Y., Fretland, J., Davidson, J.P., Billedeau, J.R., Gleason, S.K., Hirschfeld, D., Kennedy-Smith, J.J., Mirzadegan, T., Roetz, R., Smith, M., Sperry, S., Suh, J.M., Wu, J., Tsing, S., Villasenor, A.G., Paul, A., Su, G., Heilek, G., Hang, J.Q., Zhou, A.S., Jernelius, J.A., Zhang, F.J., Klumpp, K., 2008. Design of annulated pyrazoles as inhibitors of HIV-1 reverse transcriptase. J. Med. Chem. 51, 7449–7458.

Tachedjian, G., Goff, S.P., 2003. The effect of NNRTIs on HIV reverse transcriptase dimerization. Curr. Opin. Investig. Drugs 4, 966–973.

Tachedjian, G., Orlova, M., Sarafianos, S.G., Arnold, E., Goff, S.P., 2001. Nonnucleoside reverse transcriptase inhibitors are chemical enhancers of dimerization of the HIV type 1 reverse transcriptase. Proc. Natl. Acad. Sci. U.S.A. 98, 7188–7193.

Thimmig, R.L., McHenry, C.S., 1993. Human immunodeficiency virus reverse transcriptase. J. Biol. Chem. 268, 16528–16536.

Tugarinov, V., Hwang, P.M., Ollerenshaw, J.E., Kay, L.E., 2003. Cross-correlated relaxation enhanced 1H[bond]13C NMR spectroscopy of methyl groups in very high molecular weight proteins and protein complexes. J. Am. Chem. Soc. 125, 10420–10428.

Unge, T., Knight, S., Bhikhabhai, R., Lovgren, S., Dauter, Z., Wilson, K., Strandberg, B., 1994. 2.2 A resolution structure of the amino-terminal half of HIV-1 reverse transcriptase (fingers and palm subdomains). Structure 2, 953–961.

Venezia, C.F., Howard, K.J., Ignatov, M.E., Holladay, L.A., Barkley, M.D., 2006. Effects of efavirenz binding on the subunit equilibria of HIV-1 reverse transcriptase. Biochemistry 45, 2779–2789.

Wang, J., Smerdon, S.J., Jager, J., Kohlstaedt, L.A., Rice, P.A., Friedman, J.M., Steitz, T.A., 1994. Structural basis of asymmetry in the human immunodeficiency virus type 1 reverse transcriptase heterodimer. Proc. Natl. Acad. Sci. U.S.A. 91, 7242–7246.

Willard, L., Ranjan, A., Zhang, H., Monzavi, H., Boyko, R.F., Sykes, B.D., Wishart, D.S., 2003. VADAR: a web server for quantitative evaluation of protein structure quality. Nucleic Acids Res. 31, 3316–3319.